analytical chemistry

pubs.acs.org/ac Article

Fabrication of a Smart Nanofluidic Biosensor through a Reversible Covalent Bond Strategy for High-Efficiency Bisulfite Sensing and Removal

Huan Chen,[‖] Liying Xu,[‖] Wei Tuo,[‖] Xiaoya Chen, Jinmei Huang, Xin Zhang, and Yao Sun*

Cite This: *Anal. Chem.* 2020, 92, 4131−4136 Read Online

ACCESS | Metrics & More | Article Recommendations | Supporting Information

ABSTRACT: Bioinspired nanochannel based biosensors have been widely applied for sensing ions, small molecules, and biomolecules. However, the low selectivity and difficulty in recycle sensing still heavily hamper their widespread applications. Herein, we designed and fabricated a nanochannel based biosensor for high-efficiency bisulfite (HSO_3^-) sensing and removal through forming a reversible covalent bond between HSO_3^- and 4-aminophenyl-phenyl-methanone (APPM). This nanofluidic biosensor displays a promising HSO_3^- selectivity with high ion rectification/gating ratio (47 and 5) and excellent reversibility and stability. Of note, the L02 cell line containing excess HSO_3^- could still maintain high vitality in the presence of such an APPM-functionalized biosensor based membrane. These results will not only help to better understand the biological function of HSO_3^- in living organisms but also inspire us to develop smart artificial nanochannel based biosensors for biological applications.

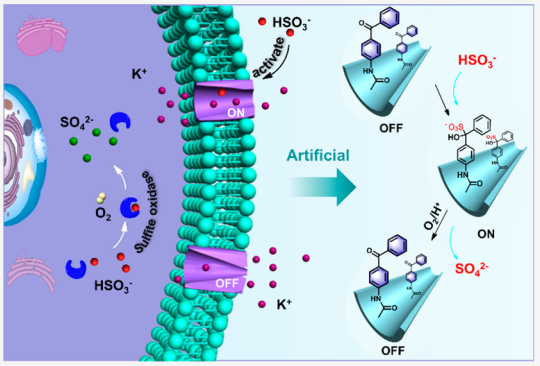

For the past several years, abnormal levels of endogenous SO_2 and its derivative bisulfite (HSO_3^-) in living organisms have been suggested to cause oxidation DNA damage and cardiovascular diseases.[1−6] It has been well documented that the mechanism can be attributed to HSO_3^- targeting the ion channels.[7−9] For example, HSO_3^- can activate the K^+ channel, thereby promoting the diffusion of K^+ ions.[10] Fortunately, the living system can spontaneously oxidize excess HSO_3^- to sulfate (SO_4^{2-}) by sulfite oxidase and excrete it from urine, thereby avoiding bisulfite-induced damage to the body.[11] Inspired by the vital role of HSO_3^- in nature, we fabricated an in vitro HSO_3^--regulated ion channel to better understand the pathological functions of bisulfites. However, the external environment easily destroys the brittle structure of the embedded lipid bilayers, which heavily restrict their practical applications.[12−19]

Owing to their outstanding stability and facile chemical properties, biomimetic nanoplatforms such as nanochannels have recently attracted broad attention from different scientific fields.[20−25] Especially, with proper functional ligand modifications, artificial nanochannels have been demonstrated to be a promising biosensor for detecting various target analytes including biomolecules, metal ions, and small molecules (including gas molecules).[26−32] The process of sensing involves several feature changes on the nanochannel based nanofluidic biosensor including surface charge, effective pore size, and wettability in the presence of target analytes, which will further impact the corresponding ion current, ion rectification, and gate state of the biosensor.[33−38] Despite these pioneer examples, most of the reported nanofluidic biosensors have so far focused primarily on hydrogen bonds and electrostatics interaction between analytes and ligands immobilized on the surface of the biosensor.[39−41] Obviously, these weak and nonspecific interactions may lead to the poor sensitivity and selectivity of the biosensors.[42−45] Recently, our group has developed a covalent bond strategy to realize the high specific and sensitive detection of Cys and NO, yet the recycling of the sensors seems to be impossible owing to the formation of an irreversible covalent bond.[46,47] Therefore, it prompts us to explore novel chemical methods to fabricate a recyclable nanofluidic biosensor with high sensitivity and selectivity for the detection and removal of toxic molecules (e.g., bisulfite).

Previous reports indicated that HSO_3^- can easily attack aldehyde or ketone groups to form bisulfite adducts (nucleophilic reaction).[48,49] Meanwhile, such bisulfite adducts can be facilely rearranged to produce the corresponding aldehydes or ketones in acidic pH conditions.[48,49] On the basis of this chemical strategy, herein, we designed and fabricated a HSO_3^--responsive nanochannel based biosensor via this

Received: January 11, 2020
Accepted: January 28, 2020
Published: January 28, 2020

https://dx.doi.org/10.1021/acs.analchem.0c00131
Anal. Chem. 2020, 92, 4131−4136

reversible covalent bond strategy (Figure 1). 4-Aminophenyl-phenyl-methanone (APPM) was immobilized on the wall of

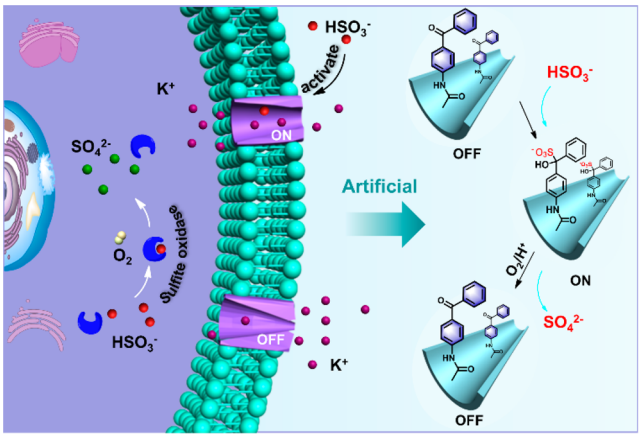

Figure 1. Schematic of a biomimetic nanochannel based biosensor for bisulfite detection and removal via a reversible covalent bond strategy.

the polyethylene terephthalate (PET) nanochannel. In this system, the ketone group of the APPM on the biosensor surface is supposed to specifically interact with HSO_3^- via a nucleophilic reaction, followed by a significant change in the hydrophilicity and an increase in the negative charge density of the biosensor surface, leading to the activation of ion transportation ("ON State"). Furthermore, the bisulfite adducts could be dissociated into the corresponding ketones in the acidic condition (pH = 3). Accordingly, the surface charge of the biosensor becomes neutral, which reduces the activity of ion transportation ("OFF State"). Therefore, this nanofluidic biosensor could exhibit both ion gating and ion current rectification tuned by HSO_3^-. Because of the formation of specific covalent bonds on its surface, this nanofluidic biosensor system overcomes the low selectivity of previous examples and displays a highly selective and sensitive HSO_3^- response without interference. More importantly, the HSO_3^--driven biosensor not only exhibits promising reversibility and stability but also is successfully applied for the efficient removal of the excess HSO_3^- in the L02 cells. These results show that this nanofluidic biosensor is promising for the biological applications of detection and removal of other toxins.

EXPERIMENTAL SECTION

Fabrication of the Nanochannel. The nanochannel was prepared in PET films using the ion track-etching technique (see Figure S8). In order to produce a single conical nanochannel, the PET membrane should be embedded between the two chambers of a conductivity cell. Then, the first chemical etching was performed from one side with an etching solution (9 M NaOH) and from the other side with a stopping solution (1 M KCl/HCOOH). During this experiment, a 1 V voltage was used to trace the etching process (20 min at 35 °C). When the current value reaches 2.5 nA, the stopping solution (1 M KCl/HCOOH) was added to both sides of the membrane for 20 min. For the second etching, the etching solution (1 M NaOH) was added to both sides. At about 2 h, when the transmembrane current reached 50 nA, the stopping solution was immediately added to neutralize the NaOH. The diameter of the base (D) verified by scanning electron microscopy (SEM) is about 400 nm, and the diameter of the tip (d_{tip}) is estimated to be about 18 nm (Supplementary Equation 1).

APPM Immobilization on the Nanochannel. As a result of chemical etching, carboxyl groups are generated on the nanochannel surface. These can be activated with 1-(3-(dimethylamino)propyl)-3-ethylcarbodiimidehydrochloride and pentafluorophenol (EDC/PFP), forming an amine-reactive ester intermediate. Then, these reactive esters were further condensed with APPM through the formation of covalent bonds. During the modification process, the PET film was first soaked in a 10 mM EDC/PFP ethanol solution for 1 h to produce amine-reactive ester molecules. Subsequently, the activated solution (EDC/PFP) was removed, and this film was washed with distilled water and treated with 10 mM APPM ethanol solution overnight. The intermediate was covalently coupled with APPM through a stable amide linkage. Finally, the modified film was washed three times with distilled water.

Ion Current Measurement. A Keithley 6487 picoammeter (Keithley Instruments, Cleveland, OH) was used to measure ion currents. The transmembrane current was identified by Ag/AgCl electrodes across the nanochannel. The $I-V$ curves were recorded via a scanning voltage signal from −2 to +2 V with a 40 s period. The average current values at different voltages were obtained through five repeated tests.

Contact Angle Measurement. Contact angles were measured using an OCA 20 system. To each sample, about 2 μL of a water droplet is dispensed onto the substrates. The average contact angle value is obtained at ten different positions of the same sample.

Finite-Element Computation. To obtain the ion concentration distribution of the APPM channel and APPM + HSO_3^- channel under experimental conditions (K^+ + Cl^-), finite-element computations based on the Poisson and Nernst−Planck equations were performed using COMSOL Multiphysics 5.3. The equations are shown in the Supporting Information. The electrolyte solution was a 0.1 M KCl solution. In COMSOL Multiphysics, the ion concentrations of K^+ and Cl^- are uniformly set to 100 mol m^{-3} and the ion diffusion coefficients of K^+ and Cl^- in bulk solution are 2.032 × 10^{-9} and 1.957 × 10^{-9} m^2/s, respectively. The simulated model is shown in Figure S6.

Cell Culture and Calcium AM/PI Staining. The L02 cell line was cultured with RPMI-1640 medium (containing 10% fetal bovine serum), 100 U/mL penicillin, and 100 μg/mL streptomycin in a cell incubator (37 °C, 5% CO_2). L02 cells were seeded into confocal dishes (NEST, China). After incubation for 12 h, different concentrations (0, 2 mM) of sodium bisulfite in RPMI-1640 (200 μL per well) were added to the plates. The control was the addition of pure culture media. For the HSO_3^- group, only sodium bisulfite in RPMI-1640 (2 mM) was added. The membrane group included the addition of sodium bisulfite in RPMI-1640 (2 mM) and the APPM biosensor. The cells were incubated for another 2 or 4 days (the medium was changed in 2 days). After treatment, the cells were incubated with Calcein-AM (1 μM) and PI (2 μM) for another 15 min and washed three times with PBS before imaging. The Calcium AM/PI double staining images were acquired using a confocal microscope (Leica TCS SP8).

MTT Assay. L02 cells were seeded into 96 well cell culture plates (1 × 10^4 per well) for 12 h in a cell incubator and treated with Calcium AM/PI double staining (cells were divided into three groups). MTT in PBS (5 mg/mL, 10 μL per well) was added, and the plates were incubated for 4 h in a cell

https://dx.doi.org/10.1021/acs.analchem.0c00131
Anal. Chem. 2020, 92, 4131−4136

incubator. DMSO (100 μL per well) was added to dissolve the formazan crystals, and the optical density value at 490 nm was measured by a microplate reader (Epoch 2, BioTek).

RESULTS AND DISCUSSION

The HSO_3^--responsive biosensor was generated from a single conical nanochannel in a polyethylene terephthalate (PET) membrane.[50] From the results of scanning electron microscopy (Figure S1) and electrochemical analysis,[51] the base/tip size was about 400 nm/18 nm. The APPM ligand was attached to the surface of the nanochannel by a traditional conjugation reaction (Figure 2a). As depicted in Figure 2b, the current−voltage (I−V) features of this nanochannel were distinguishably different before and after immobilization with APPM. The ion rectification ratio was calculated by the absolute values of the ion currents at a given voltage (−2 V versus +2 V). The unmodified nanochannel at a neutral pH (0.1 M KCl) was negatively charged due to the presence of free −COOH groups, leading to a high ion current rectification ratio (~20, Figure S2). After conjugation with APPM, the negative charge of the nanochannel was significantly reduced, causing a remarkable decrease in the ion current rectification ratio (~4). To further verify the successful construction of the biosensor, the wettability and chemical composition of the nanochannel before and after immobilization with APPM were characterized by contact angle (CA)/X-ray photoelectron spectroscopy measurements (Figure 2b,c and Tables S1 and S2). Obviously, functionalization of the nanochannel with APPM causes a significant change in the CA (from 58.9 ± 1.5° to 92.5 ± 1.6°). A new N peak at ~400 eV appeared after the APPM modification in the XPS analysis (Figure 2c). Moreover, laser scanning confocal microscopy (LSCM) also revealed a strong fluorescence signal for the APPM-functionalized biosensor (Figure 2d).

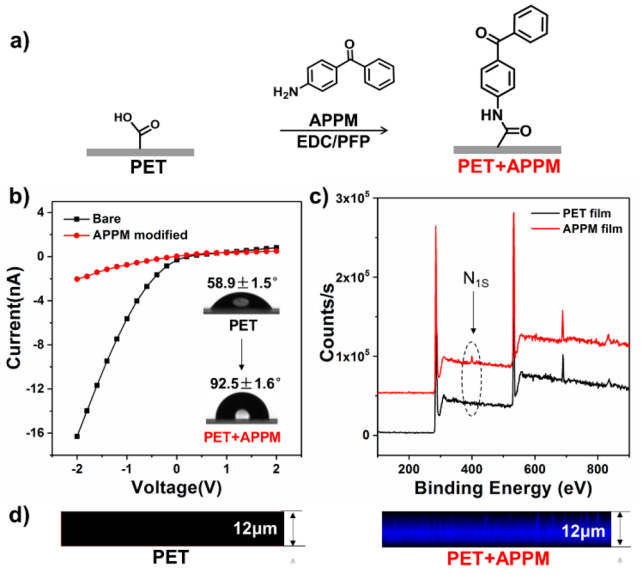

Figure 2. (a) Fabrication of the HSO_3^--driven biosensor based on the PET nanochannel. (b) I−V features of the nanochannel based biosensor before and after APPM modification in 0.1 M KCl. (c) XPS analysis of the nanochannel based biosensor before and after APPM modification. (d) Laser scanning confocal microscopy (LSCM) images of the nanochannel based biosensor before and after APPM modification.

The HSO_3^- sensing ability of the nanofluidic biosensor was then investigated. As illustrated in Figure 3a, the I−V features of the biosensor displayed an obviously rectified behavior after treatment with HSO_3^-. Meanwhile, the calculated rectification ratio of the APPM-functionalized biosensor in the presence of HSO_3^- was much higher than that in the absence of HSO_3^- (47 vs 4, defined as $I_R = I_{-2\ V}/I_{+2\ V}$, Figure 3b). A new S_{2p} peak at ~162.28 eV appeared after adding HSO_3^- from the result of the XPS analysis, which also verified the successful modification (Figure S3 and Tables S2 and S3). Moreover, it suggested that the rectified behavior of the I−V curve was gradually enhanced as a result of the increasing HSO_3^- concentration (from 10^{-6} to 5×10^{-3} M), and the APPM-functionalized biosensor was still able to respond well to HSO_3^- even at a concentration as low as 5 μM (Figure 3c). In addition, the alteration of the gating ratio at −2 V (defined as $Rg = (I - I_0)/I_0$, where I_0 and I are the currents measured at −2 V in the absence and presence of HSO_3^-, respectively) caused by different concentrations of HSO_3^- was also investigated. The gating ratio of the APPM-functionalized biosensor was dramatically increased (up to 5) with the enhancement of HSO_3^- concentration and reached a saturation when the concentration was about 1 mM (Figure 3d). Furthermore, the gating ratio and the logarithm of the concentration showed a positive correlation (Figure S4). The HSO_3^- responsive rate of the APPM-functionalized biosensor was also determined on the basis of I−T curves. Figure S5 illustrated the low concentration of HSO_3^- (10^{-6} M) only slightly influenced the current change of the biosensor. When the HSO_3^- concentration increased, the corresponding current of the biosensor gradually decreased. Moreover, the biosensor can rapidly detect HSO_3^- at a concentration of 1 mM, and the ionic current did not decay (>30 s) due to the saturated binding between APPM and HSO_3^-.

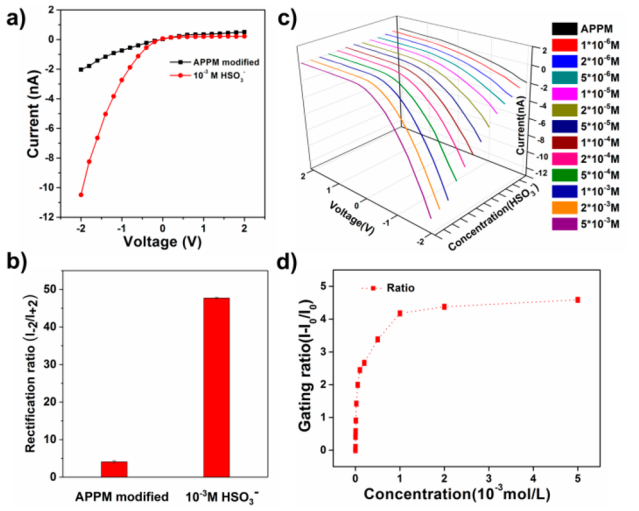

Figure 3. (a) I−V features of the APPM-functionalized biosensor in the absence and presence of HSO_3^- (0.1 M KCl). (b) The rectification ratio of the APPM-functionalized biosensor in the absence and presence of HSO_3^-. (c) I−V features of the APPM-functionalized biosensor in 0.1 M KCl upon the addition of different concentrations of HSO_3^-. (d) The dynamic changes on the gating ratios of the APPM-functionalized biosensor upon the addition of 1 mM HSO_3^-.

https://dx.doi.org/10.1021/acs.analchem.0c00131
Anal. Chem. 2020, 92, 4131−4136

In order to demonstrate the selectivity of this APPM-functionalized biosensor, it was treated with various substrates (i.e., NO_3^-, SO_4^{2-}, HCO_3^-, Br^-, I^-, H_2O_2, and HSO_3^-) for 5 min. As depicted in Figure 4a, both the gating ratio and rectification ratio of HSO_3^- were dramatically higher than those of other substrates, further confirming the high selectivity and specificity of the biosensor for HSO_3^-. This could be attributed to the fact that HSO_3^- rather than other substrates specifically reacted with the APPM ligand, followed by altering the surface charge of the APPM-functionalized biosensor. Furthermore, the switchable ability of this biosensor was evaluated by recording current (−2 V) changes in the presence of HSO_3^-. As seen in Figure 4b, the biosensor surface was negatively charged after adding HSO_3^-, which resulted in a low resistance and an increase in ion current. Hence, the gate was in the ON state for K^+ selective transport. After the pH was adjusted to 4, the current at −2 V markedly decreased to −2.0 nA owing to the HSO_3^- removal from the surface of the APPM-functionalized biosensor. Therefore, the surface of the biosensor changed to be positively charged, and the gate showed the OFF state for K^+ transport. After repeating the process five times, no damping of the ion current was observed, which indicated that the APPM-functionalized biosensor displayed promising switchability and stability. Meanwhile, the reversible changes on the contact angle (CA) from 63.7 ± 2.5° to 92.5 ± 1.6° also revealed the HSO_3^- and acidic pH-involved regulation process (Figure 4c).

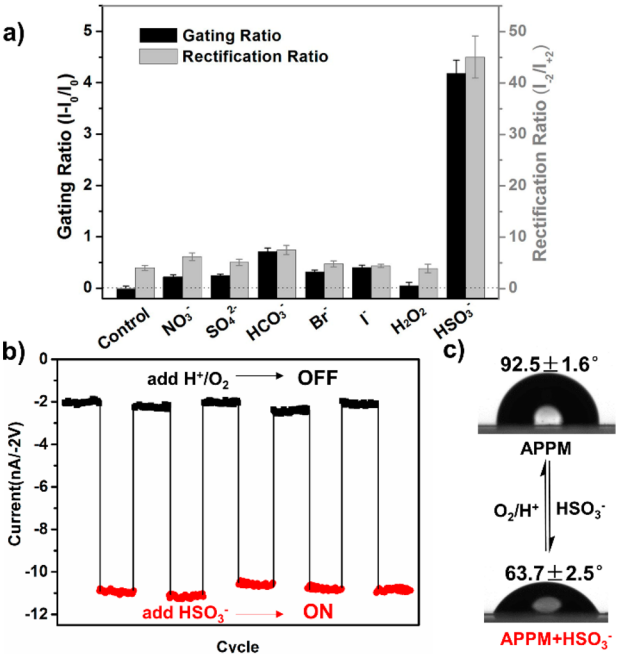

Figure 4. (a) Gating ratios and rectification ratios measured in 0.1 M KCl upon the addition of different substrates. (b) The recyclability of the HSO_3^-/pH-regulated APPM-functionalized biosensor. (c) The switchability of the water droplet shape on the APPM-functionalized PET films under the HSO_3^- and acidic pH conditions.

various cell lines.[52] Immunofluorescence analysis (Calcein-AM and PI staining) was applied to investigate the living state of cells containing excess bisulfite (2 mM) in the presence or absence of an APPM-functionalized membrane. The L02 cell line was chosen and divided into three groups: culture medium with the addition of bisulfite (named the HSO_3^- group), with the addition of the bisulfite/APPM-biosensor membrane (named the membrane group), and without the addition of bisulfite (named the control group). As displayed in Figure 5a,

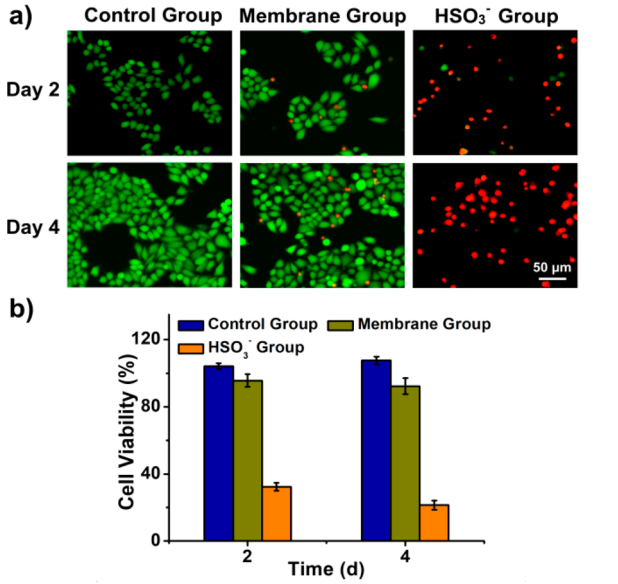

Figure 5. (a) Fluorescence images of live/dead L02 cells (green/red) with Calcein-AM and PI staining after various treatments. (b) Cell viabilities under various treatments.

the cell viabilities of the control group and the membrane group were negligibly affected. However, almost all cells in the bisulfite group were dead after 2 days of culture, which suggested that the addition of the APPM-functionalized biosensor membrane could efficiently protect L02 cells from bisulfite-induced apoptosis. Moreover, the membrane group showed significantly higher cell proliferation and vitality than the HSO_3^- group in the MTT assay (Figure 5b). Hence, the APPM-functionalized biosensor membrane can efficiently eliminate excess bisulfite from living cells and maintain the vitality and proliferation of the cells.

Finally, we attempted to elucidate the potential mechanism of HSO_3^--mediated K^+ transport through the APPM-functionalized biosensor. Finite-element computations were performed on the basis of the Poisson and Nernst−Planck equations by COMSOL Multiphysics 5.3 to reveal the behavior of ions in the biosensor with a corresponding charge density.[53] Figure 6a illustrated the 2D profile of ion concentration at −2 V. The ion concentration on the negatively charged surface of the biosensor (simulation of the APPM-functionalized biosensor) seemed to be higher than that on the neutral surface as a result of K^+ enrichment. The ion enrichment due to the overlap of the electric double layer at the tip side of the negatively charged biosensor resulted in the generation of high ion conductance as well as high ionic current. Therefore, HSO_3^- causes polarity conversion of the surface charge, followed by switching the gate state of the biosensor from OFF to ON (for details, see the Experimental Section and Figure S6). The

https://dx.doi.org/10.1021/acs.analchem.0c00131
Anal. Chem. 2020, 92, 4131−4136

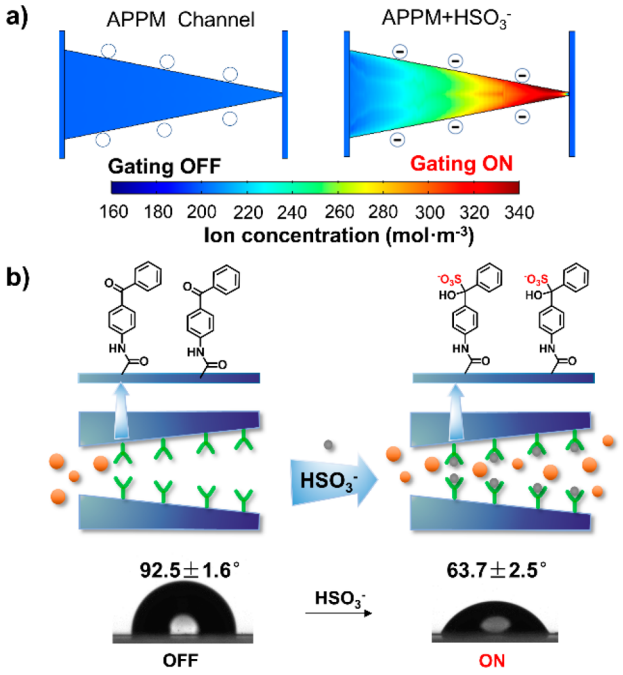

Figure 6. (a) Numerical simulation of the ion concentration (total of K^+ and Cl^-) distribution in the biosensor (at −2 V, with 0.1 M KCl). (b) The surface chemical structure of the APPM-functionalized biosensor.

significant transformation of the surface charge and the change in chemical structure were attributed to the nucleophilic reaction between APPM and HSO_3^- (Figure 6b). The electrospray ionization-mass spectrometry (ESI-MS) analysis also confirmed the HSO_3^--regulated process involving the nucleophilic reaction in solution (Figure S7). In addition to the charge regulation, wettability is also involved in the regulation process. The CA changes from 92.5 ± 1.6° to 63.7 ± 2.5° reflect the wettability change of the channel surface (Figure 6b). The electrolyte solution easily enters hydrophilic nanochannels to facilitate ion transport. Therefore, the increase in the hydrophilicity caused by the addition of HSO_3^- switches the gate state of the biosensor from OFF to ON. As a summary of the mechanism, the HSO_3^--regulated chemical structure change in the APPM-functionalized biosensor leads to changes in the surface charge from neutral to negative; accordingly, the negatively charged APPM-functionalized biosensor showed higher ion conductance and greater ion transmission compared to before, which is regarded as the ON state of the ionic gating.

CONCLUSIONS

In summary, we have successfully fabricated an APPM-functionalized biosensor with promising HSO_3^- selectivity, gating, and recyclable properties. On the basis of this reversible covalent bond strategy, such a biosensor exhibits promising reversibility and stability as well as high efficiency in removing excess HSO_3^- from L02 cells. These results make this nanochannel based biosensor helpful and useful in potential biological applications, such as understanding the biological function of HSO_3^- in living organisms and removing endogenous toxins.

ASSOCIATED CONTENT

Supporting Information

The Supporting Information is available free of charge at https://pubs.acs.org/doi/10.1021/acs.analchem.0c00131.

SEM image; rectification ratio of bare and APPM channels; XPS data; linear relationship of gating ratio and logarithm of concentration; dynamic regulation process; model of numerical simulation; ESI-MS analysis; device diagram for the etching process; additional experimental details (PDF)

AUTHOR INFORMATION

Corresponding Author

Yao Sun − *Key Laboratory of Pesticides and Chemical Biology, Ministry of Education, International Joint Research Center for Intelligent Biosensor Technology and Health, Center of Chemical Biology, College of Chemistry, Central China Normal University, Wuhan, Hubei 430079, China;* orcid.org/0000-0002-6519-7436; Email: sunyaogbasp@mail.ccnu.edu.cn

Authors

Huan Chen − *Key Laboratory of Pesticides and Chemical Biology, Ministry of Education, International Joint Research Center for Intelligent Biosensor Technology and Health, Center of Chemical Biology, College of Chemistry, Central China Normal University, Wuhan, Hubei 430079, China; Ministry of Education Key Laboratory for the Synthesis and Application of Organic Functional Molecules, Hubei University, Wuhan, Hubei 430062, China*

Liying Xu − *Department of Radiology, Zhongnan Hospital of Wuhan University, Wuhan, Hubei 43007, China*

Wei Tuo − *Department of Chemistry, University of Utah, Salt Lake City, Utah 84112, United States*

Xiaoya Chen − *CAS Key Laboratory of Nano-Bio Interface, Suzhou Institute of Nano-Tech and Nano-Bionics, Chinese Academy of Sciences, Suzhou, Jiangsu 215123, China*

Jinmei Huang − *Key Laboratory of Pesticides and Chemical Biology, Ministry of Education, International Joint Research Center for Intelligent Biosensor Technology and Health, Center of Chemical Biology, College of Chemistry, Central China Normal University, Wuhan, Hubei 430079, China*

Xin Zhang − *Key Laboratory of Pesticides and Chemical Biology, Ministry of Education, International Joint Research Center for Intelligent Biosensor Technology and Health, Center of Chemical Biology, College of Chemistry, Central China Normal University, Wuhan, Hubei 430079, China*

Complete contact information is available at: https://pubs.acs.org/10.1021/acs.analchem.0c00131

Author Contributions

‖H.C., L.X., and W.T. contributed equally to this work.

Notes

The authors declare no competing financial interest.

ACKNOWLEDGMENTS

This work was supported by the National Natural Science Foundation of China (21708012) Wuhan scientific and technological projects (2019020701011441) and NSFHP (2017CFB151). Finally, we thank the Open Research Fund supported by Ministry-of-Education Key Laboratory for the Synthesis and Application of Organic Functional Molecules, Hubei University (KLSAOFM1809), and the Open Research

https://dx.doi.org/10.1021/acs.analchem.0c00131
Anal. Chem. 2020, 92, 4131−4136

Fund supported by CAS Key Laboratory of Nano-Bio Interface (NO:19NBI01).

REFERENCES

(1) Calvert, J. W.; Jha, S.; Gundewar, S.; Elrod, J. W.; Ramachandran, A.; Pattillo, C. B.; Kevil, C. G.; Lefer, D. J. *Circ. Res.* **2009**, *105*, 365.
(2) Woerman, A. L.; Mendelowitz, D. *Cardiovasc. Res.* **2013**, *99*, 16.
(3) Zhou, X.; Lee, S.; Xu, Z.; Yoon, J. *Chem. Rev.* **2015**, *115*, 7944.
(4) Wu, L.; Sun, Y.; Sugimoto, K.; Luo, Z.; Ishigaki, Y.; Pu, K.; Suzuki, T.; Chen, H.; Ye, D. *J. Am. Chem. Soc.* **2018**, *140*, 16340.
(5) Li, Y.; Shu, Y.; Liang, M.; Xie, X.; Jiao, X.; Wang, X.; Tang, B. *Angew. Chem., Int. Ed.* **2018**, *57*, 12415.
(6) Liu, H.; Chen, L.; Xu, C.; Li, Z.; Zhang, H.; Zhang, X.; Tan, W. *Chem. Soc. Rev.* **2018**, *47*, 7140.
(7) Yu, W.; Jin, H.; Tang, C.; Du, J.; Zhang, Z. *Br. J. Pharmacol.* **2018**, *175*, 1114.
(8) Zhang, Q.; Tian, J.; Bai, Y.; Lei, X.; Li, M.; Yang, Z.; Meng, Z. *Eur. J. Pharmacol.* **2014**, *742*, 31.
(9) Meng, Z.; Li, Y.; Li, J. *Arch. Biochem. Biophys.* **2007**, *467*, 291.
(10) Zhang, Q.; Meng, Z. *Eur. J. Pharmacol.* **2009**, *602*, 117.
(11) Stipanuk, M. H. *Annu. Rev. Nutr.* **1986**, *6*, 179.
(12) Zhang, Z.; Wen, L.; Jiang, L. *Chem. Soc. Rev.* **2018**, *47*, 322.
(13) Duan, R.; Lou, X.; Xia, F. *Chem. Soc. Rev.* **2016**, *45*, 1738.
(14) Zhu, Y.; Zhan, K.; Hou, X. *ACS Nano* **2018**, *12*, 908.
(15) Wang, M.; Meng, H.; Wang, D.; Yin, Y.; Stroeve, P.; Zhang, Y.; Sheng, Z.; Chen, B.; Zhan, K.; Hou, X. *Adv. Mater.* **2019**, *31*, 1805130.
(16) Howorka, S.; Siwy, Z. *ACS Nano* **2016**, *10*, 9768.
(17) Ying, Y.; Long, Y. *J. Am. Chem. Soc.* **2019**, *141*, 15720.
(18) Si, W.; Xin, P.; Li, Z.; Hou, J. *Acc. Chem. Res.* **2015**, *48*, 1612.
(19) Zhao, X.; Zhou, Y.; Zhang, Q.; Yang, D.; Wang, C.; Xia, X. *Anal. Chem.* **2019**, *91*, 1185.
(20) Cao, C.; Long, Y. *Acc. Chem. Res.* **2018**, *51*, 331.
(21) Shen, J.; Li, Y.; Gu, H.; Xia, F.; Zuo, X. *Chem. Rev.* **2014**, *114*, 7631.
(22) Sheng, Z.; Wang, H.; Tang, Y.; Wang, M.; Huang, L.; Min, L.; Meng, H.; Chen, S.; Jiang, L.; Hou, X. *Sci. Adv.* **2018**, *4*, No. eaao6724.
(23) Xin, W.; Zhang, Z.; Huang, X.; Hu, Y.; Zhou, T.; Zhu, C.; Kong, X.; Jiang, L.; Wen, L. *Nat. Commun.* **2019**, *10*, 3876.
(24) Zhu, Z.; Zheng, S.; Peng, S.; Zhao, Y.; Tian, Y. *Adv. Mater.* **2017**, *29*, 1703120.
(25) Lin, L.; Liu, Y.; Yan, J.; Wang, X.; Li, J. *Anal. Chem.* **2013**, *85*, 334.
(26) Hou, X.; Siwy, Z.; Ulbricht, M. *Small* **2018**, *14*, 1800908.
(27) Perez-Mitta, G.; Toimil-Molares, M. E.; Trautmann, C.; Marmisolle, W.; Azzaroni, O. *Adv. Mater.* **2019**, *31*, 1901483.
(28) Xiao, K.; Chen, L.; Zhang, Z.; Xie, G.; Li, P.; Kong, X.; Wen, L.; Jiang, L. *Angew. Chem., Int. Ed.* **2017**, *56*, 8168.
(29) Li, X.; Zhai, T.; Gao, P.; Cheng, H.; Hou, R.; Lou, X.; Xia, F. *Nat. Commun.* **2018**, *9*, 2617.
(30) Chen, S.; Tang, Y.; Zhan, K.; Sun, D.; Hou, X. *Nano Today* **2018**, *20*, 84.
(31) Perez-Mitta, G.; Albesa, A. G.; Trautmann, C.; Toimil-Molares, M. E.; Azzaroni, O. *Chem. Sci.* **2017**, *8*, 890.
(32) Lin, L.; Yan, J.; Li, J. *Anal. Chem.* **2014**, *86*, 10546.
(33) Sun, Y.; Zhang, F.; Quan, J.; Zhu, F.; Hong, W.; Ma, J.; Pang, H.; Sun, Y.; Tian, D.; Li, H. *Nat. Commun.* **2018**, *9*, 2617.
(34) Sun, Y.; Ma, J.; Zhang, F.; Zhu, F.; Mei, Y.; Liu, L.; Tian, D.; Li, H. *Nat. Commun.* **2017**, *8*, 260.
(35) Zhu, Z.; Wang, D.; Tian, Y.; Jiang, L. *J. Am. Chem. Soc.* **2019**, *141*, 8658.
(36) Zhang, Q.; Kang, J.; Xie, Z.; Diao, X.; Liu, Z.; Zhai, J. *Adv. Mater.* **2018**, *30*, 1703323.
(37) Ali, M.; Tahir, M. N.; Siwy, Z.; Neumann, R.; Tremel, W.; Ensinger, W. *Anal. Chem.* **2011**, *83*, 1673.
(38) Zhang, F.; Ma, J.; Sun, Y.; Mei, Y.; Chen, X.; Wang, W.; Li, H. *Anal. Chem.* **2018**, *90*, 8270.
(39) Hou, X. *Adv. Mater.* **2016**, *28*, 7049.
(40) Ali, M.; Yameen, B.; Cervera, J.; Ramirez, P.; Neumann, R.; Ensinger, W.; Knoll, W.; Azzaroni, O. *J. Am. Chem. Soc.* **2010**, *132*, 8338.
(41) Long, Z.; Zhan, S.; Gao, P.; Wang, Y.; Lou, X.; Xia, F. *Anal. Chem.* **2018**, *90*, 577.
(42) Xu, Y.; Sui, X.; Jiang, J.; Zhai, J.; Gao, L. *Adv. Mater.* **2016**, *28*, 10780.
(43) Xu, Y.; Sui, X.; Guan, S.; Zhai, J.; Gao, L. *Adv. Mater.* **2015**, *27*, 1851.
(44) Sun, Y.; Zhang, F.; Sun, Z.; Song, M.; Tian, D.; Li, H. *Chem. - Eur. J.* **2016**, *22*, 4355.
(45) Zhang, R.; Chen, X.; Sun, Z.; Chen, S.; Gao, J.; Sun, Y.; Li, H. *Anal. Chem.* **2019**, *91*, 6149.
(46) Sun, Z.; Han, C.; Song, M.; Wen, L.; Tian, D.; Li, H.; Jiang, L. *Adv. Mater.* **2014**, *26*, 455.
(47) Sun, Y.; Chen, S.; Chen, X.; Xu, Y.; Zhang, S.; Ouyang, Q.; Yang, G.; Li, H. *Nat. Commun.* **2019**, *10*, 1323.
(48) Lin, V. S.; Chen, W.; Xian, M.; Chang, C. J. *Chem. Soc. Rev.* **2015**, *44*, 4596.
(49) Zuman, P. *Chem. Rev.* **2004**, *104*, 3217.
(50) Wang, Y.; Zhai, J. *Langmuir* **2019**, *35*, 3171.
(51) Kalman, E. B.; Vlassiouk, I.; Siwy, Z.; et al. *Anal. Bioanal. Chem.* **2009**, *394*, 413.
(52) Beckman, K. B.; Ames, B. N. *J. Biol. Chem.* **1997**, *272*, 19633.
(53) Xiao, K.; Xie, G.; Zhang, Z.; Kong, X.; Liu, Q.; Li, P.; Wen, L.; Jiang, L. *Adv. Mater.* **2016**, *28*, 3345.

https://dx.doi.org/10.1021/acs.analchem.0c00131
Anal. Chem. 2020, 92, 4131−4136